Spin-torch experiment on reaction centers of Rhodobacter sphaeroides

Sai Sankar Gupta, K.B.

Chapter 4

Characterization of bacteriopheophytin *a* in the active branch of the reaction center of *Rhodobacter sphaeroides* by ^{13}C photo-CIDNP MAS NMR

Abstract

The electronic structure of the primary electron acceptor, bacteriopheophytin *a* (Φ_A), in photosynthetic reaction centers (RCs) of the purple bacterium *Rhodobacter (R.) sphaeroides* is investigated by photochemically induced dynamic nuclear polarization (photo-CIDNP) magic-angle spinning (MAS) NMR spectroscopy. Uniformly labelled RCs have been prepared for these experiments, by adding the u-$^{13}C_4$-δ-aminolevulinic acid as a precursor in the growing medium of *R. sphaeroides* wild type (WT). By using assignments from different selective labelling patterns, the ^{13}C observed chemical shifts attributed to the Φ_A have been compiled. These assignments are supported by theoretical calculations of ^{13}C chemical shifts of a bacteriopheophytin in two conformations, a fully relaxed geometry and in the x-ray structure found for Φ_A. The relative electronic densities of Φ_A in the ground state have been obtained by comparing these assignments with those of free bacteriopheophytin in acetone solution. From that analysis, it can be concluded that Φ_A in the active branch is not tuned in a special manner by its surrounding and appears to be electronically close to free bacteriopheophytin.

4.1 Introduction

Natural photosynthesis achieves the conversion of solar energy with a remarkably small set of cofactors, and the functional programming of the pigment chromophores is to a large extent encoded by their conformation, local environment, dynamics and mutual interactions. The photosynthetic apparatus of plants, algae and bacteria contain densely packed pigment-pigment and pigment-protein complexes for harvesting light and separating electrons and protons across the photosynthetic membrane (for reviews, (Hoff & Deisenhofer, 1997; Hunter *et al.*, 2008)). Both the photosynthetic reaction centers (RCs) and the light harvesting antennae of the purple bacterium *Rhodobacter (R.) sphaeroides* contain networks of interacting bacteriochlorophyll BChl *a*. In the RC, four BChl *a* and two bacteriopheophytin (BPhe) *a* are positioned in an apparent symmetric arrangement and use the energy absorbed by the BChls in LH2 and LH1 light harvesting antennae complexes. Two BChl *a* form an interacting dimer called the "Special Pair" (P). On either side of the special pair an additional BChl *a* molecule is located, the accessory BChls (B_A and B_B). In addition, two BPhe (Φ) are positioned at an edge-to-edge distance of ~14 Å from the special pair (Yeates *et al.*, 1988; Ermler *et al.*, 1994; Camara-Artigas *et al.*, 2002b).

Despite an approximate global symmetry in the arrangement of these six cofactors, their functioning is asymmetric, since charge separation proceeds almost exclusively over the A-branch. When excitations from the antennae are trapped by the special pair in the RCs, quantum delocalization by electron tunneling from the P* into the B_A and then into the Φ_A, leads to symmetry breaking of the excited state to establish the consecutive charge transfer contributions $P^+B_A^-$ and $P^+\Phi_A^-$. Hence, for the RC of *R. sphaeroides*, the charge transfer proceeds along the redox gradient represented by the cofactors of the A branch, and the functional mechanisms of this electron transfer process have been well studied. EPR, ENDOR and optical methods have provided insight into the electronic and spatial structure of the Special Pair donor and have clarified the role of the accessory BChls in the ET reaction (Feher *et al.*, 1972; Lubitz *et al.*, 1985; Shkuropatov & Shuvalov, 1993;

Schmidt *et al.*, 1994; Holzwarth & Muller, 1996; Franken *et al.*, 1997a, b; Lubitz & Feher, 1999; Moore *et al.*, 1999). The two halves of P are bound to the L and M subunits of the protein complex. MAS NMR in the dark and with photo-CIDNP enhancement has revealed packing effects on the cofactors induced by the folding and self-assembly of the RC complex. These packing effects produce structural deformation and electrostatic polarization of the BChl macrocycles and lead to electronic asymmetry of the form $P_L^{\delta-}P_M^{\varepsilon-}$ between the two BChl *a* of the P, (Prakash *et al.*, 2007; Alia *et al.*, 2009; Daviso *et al.*, 2009c; Wawrzyniak *et al.*, 2011). The variation of chemical shifts, also relative to the ^{13}C responses of BChl *a* in solution, cannot be explained by local side chain interactions, such as hydrogen bonding or nonplanarity of the $C3^1$ acetyl, but appears to be dominated by protein-induced macrocycle distortion (Daviso *et al.*, 2009c; Wawrzyniak *et al.*, 2011). Shaping of the macrocycle prominently affects the site energies, and this allows for dynamic structural tuning of the energy levels of the BChls by photosynthetic protein complexes (Daviso *et al.*, 2009c; Pandit *et al.*, 2010; Wawrzyniak *et al.*, 2011). In addition, ^{15}N and ^{13}C NMR data and DFT calculations have revealed an asymmetric electronic environment of P, which can facilitate thermodynamic control over the rate and direction of electron transfer (Alia *et al.*, 2009; Wawrzyniak *et al.*, 2011). Light enhanced DARR correlation spectroscopy of dynamic measurements in the ground state has shown that the protein environment induces strain on the BChls of P. The pair of BChls is subject to thermally activated dynamics along a few specific soft collective vibrational modes, which may lead to polymorphism in crystallization experiments and explain the inhomogeneous broadening of the optical absorption at ambient temperature (Huber *et al.*, 1998). The special pair dynamics is asymmetric, it is restricted to the overlap region formed by the rings I of the P_L and the P_M, and most of the dynamics is in the P_M (Chapter.2).

The excitation of P causes a change in the shape of P and its environment (Friesner & Won, 1989). The localized dynamics initiates directional charge transfer character in the special pair at the first stage of the photochemistry by symmetry breaking of excitons and increasing the polaronic character, leading to a

$P_L^+P_M^-$ charge transfer contribution to the product state (Moore *et al.*, 1999). The rate of formation of the $P^+\Phi_A^-$ primary product state depends on its free energy level relative to the $P^+B_A^-$ intermediate. When BPhe *a* is replaced by plant pheophytin *a* with a more negative redox potential, the free energy level of $P^+\Phi_A^-$ is ~ 200 cm^{-1} above $P^+B_A^-$, and this slows down the forward electron transfer (Franken *et al.*, 1997a, b). For such pheophytin-modified RCs of *R. sphaeroides* R-26, a coupling to collective nuclear modes in the development on the excited state potential energy surface leads to classically coherent control over the quantum delocalization in the formation of the charge separated states $P^+B_A^-$, $P^+\Phi_A^-$, and this has helped to resolve the mechanism of symmetry breaking in the first steps of the charge separation processes (Shuvalov & Yakovlev, 2003).

In contrast with the Marcus theory of electron transfer, the charge separation dynamics is apparently not coupled to random thermal motion in many nuclear modes (Marcus, 1956a, b, 1965). The strength of the coherence primarily depends on the displacement along two collective nuclear modes, an intradimer mode of around 130 cm^{-1} and a low frequency mode of ~32 cm^{-1} that is attributed to reorganization of a water molecule (Yakovlev *et al.*, 2002). This H_2O is hydrogen bonded to the B_A ring V keto functionality and the N_π of the HisM202 that is axially coordinated with its N_τ to the Mg^{2+} of the P_M. According to DFT modeling guided by MAS NMR data, this structural motif can stabilize a $P^+B_A^-$ charge transfer contribution by a release of free energy (Alia *et al.*, 2009; Wawrzyniak *et al.*, 2011). The 130 cm^{-1} collective mode is connected with the intermolecular dynamics within the special pair and its histidine ligands that develop the $P_L^+P_M^-$ charge transfer character upon excitation of the RC. Via the partially charged and polarizable His and the H_2O, the change in magnitude and angle upon excitation of the electric dipole moment of P that is governed by the intradimer displacement along the 130 cm^{-1} reaction coordinate can be coupled to $P^+B_A^-$ charge transfer, initially without a large structural displacement in the H_2O bridge (Alia *et al.*, 2009; Wawrzyniak *et al.*, 2011).

According to a recent Redfield density matrix analysis of a phenomenological model of the RC, comprising the P* and the $P^+B_A^-$ diabatic states strongly coupled to two modes, the electron transfer proceeds only after some passages through the crossing point of the P* and the $P^+B_A^-$ energy levels, by the displacement along the second reaction coordinate, the 32 cm^{-1} collective mode that is thought to be connected with the rotation of the water molecule . Thus, there is converging evidence that efficient photoproduct formation in a few picoseconds in the first steps of charge separation with a high forward transfer rate and a low probability for back transfer requires the combined displacement along a few selective vibrational modes coupled to symmetry breaking and charge transfer.

Thus, photosynthetic RC complexes represent complex dynamic topologies to promote charge separation on the excited state surface by easily accessible transition states and well-defined reaction coordinates for proceeding from the reactant to the product configurations $P_L^+P_M^-$ and $P^+B_A^-$. However, full charge separation requires transfer of an electron to the primary acceptor Φ_A to form the donor-acceptor radical pair state $P^+\Phi_A^-$ (Martin *et al.*, 1986).

The purpose of this study is to investigate by photo-CIDNP MAS NMR, the extent of functional preprogramming of the Φ_A, in its ground state, by charging, conformational tuning, or strain that produces thermal activation in specific modes. The discovery of the solid-state photo-CIDNP effect for *R. sphaeroides* R26 RCs under continuous illumination with white light, offers NMR access to the electronic and spatial structure of both the donor and the acceptor in the primary charge separation process (Zysmilich & McDermott, 1994). By induction of a non-Boltzmann nuclear spin polarization upon photoreaction in rigid samples, a signal enhancement of a factor of more than 10,000 has been observed by ^{13}C MAS NMR in several RCs (Prakash *et al.*, 2005; Prakash *et al.*, 2006; Roy *et al.*, 2008). The method is rapidly evolving, and solid-state photo-CIDNP is now routinely observed for virtually all types of photosynthetic RCs, including those of purple bacteria of *R. sphaeroides* wildtype (WT) (Prakash *et al.*, 2005) and of

Rhodopseudomonas acidophila (Diller *et al.*, 2008) of the green sulphur bacterium *Chlorobium tepidum* (Roy *et al.*, 2007), of the heliobacterium *Heliobacillus mobilis* (Roy *et al.*, 2008) as well as of the photosystems I and II of plants (Matysik *et al.*, 2000a; Alia *et al.*, 2004; Diller *et al.*, 2007a) and algae (Janssen *et al.*, 2010). The occurrence of the solid-state photo-CIDNP effect is an intrinsic property of natural photosynthetic RCs and Photo-CIDNP is a good method to resolve the local spatial and electronic structure both the donor and the acceptor, thereby providing access to intimate details of how the $P^{+}\Phi_{A}^{-}$ state is involved in the cascade of symmetry breaking mechanisms (Matysik *et al.*, 2009).

4.2 Materials and Method

4.2.1 Sample Preparation and specific isotopic labelling

The isotope labelling of cofactors in RCs is achieved by using labelled δ-aminolevulinic acid (ALA) that acts as a precursor for the biosynthesis of BChl and BPhe (Jordan, 1991; Matysik *et al.*, 2001). By enriching the growth medium with (u-^{13}C)-ALA labelled substrate, RCs that are labelled in the macroaromatic cycles of the cofactors are produced (Figure 4.1). The RCs were isolated as described previously (Shochat *et al.*, 1994). Quinones were removed by incubating the RCs at a concentration of 0.6 µM in 4% LDAO, 10 mM *o*-phenanthroline, 10 mM Tris buffer, pH 8.0, containing 0.025% LDAO and 1 mM EDTA (Okamura *et al.*, 1975).

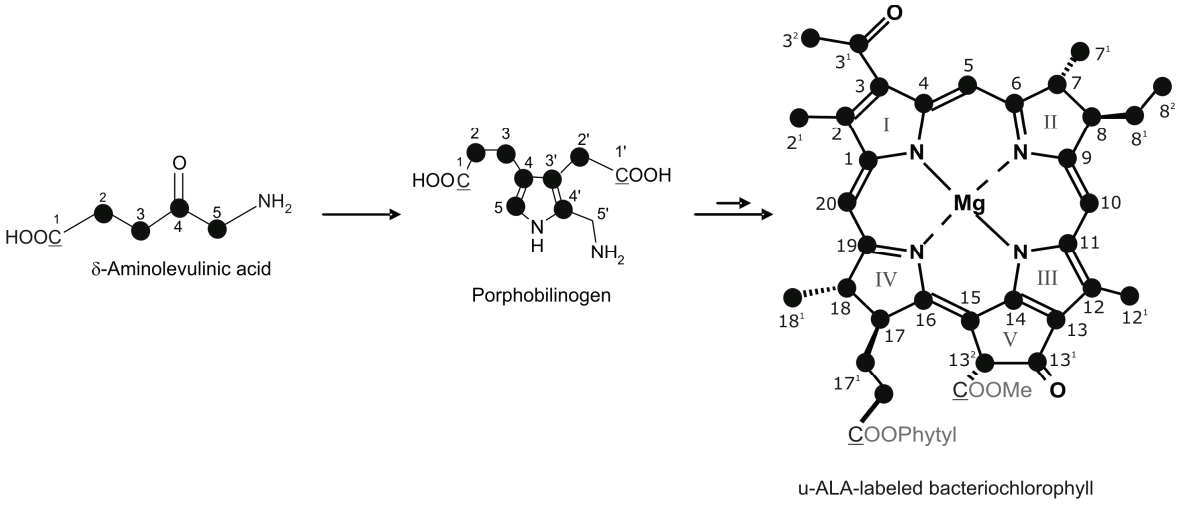

Figure 4.1 Biosynthetic pathway for the formation of selectively ^{13}C isotope labelled bacteriocholorophyll *a* (BChl) by feeding the bacteria with u-$^{13}C_4$-δ-aminolevulinic acid (u-ALA).

Approximately 15 mg of RC protein complex embedded in LDAO micelles was used for NMR experiments. Similarily with selective labeling of δ-aminolevulinic acid at different positions namely 3-^{13}C-ALA (chapter 3), 4-^{13}C-ALA (Daviso *et al.*, 2009a) and 5-^{13}C-ALA (Prakash *et al.*, 2007) RC's with sparse labeling in the cofactor rings were prepared (see: Figures in Appendix-A).

4.2.2 MAS-NMR experiments

NMR experiments were performed with an Avance DMX-200 NMR spectrometer equipped with a MAS probe (Bruker, Karlsruhe, Germany). The sample was loaded into a clear 4-mm sapphire rotor, inserted into the MAS probe and frozen slowly at a low spinning frequency of 600 Hz to ensure a homogeneous sample distribution against the rotor wall (Fischer *et al.*, 1992) . The light and dark spectra were collected with a Hahn echo pulse sequence with the CYCLOPS phase cycle of the (π/2) pulse and detection under proton decoupling using the TPPM sequence (Bennett *et al.*, 1995) at a temperature of 223 K under continuous illumination with white light (Matysik *et al.*, 2001). The optimum length of the (π /2) carbon pulse, determined on uniformly ^{13}C labelled tyrosine, is ~4 μs under our experimental conditions using a rf strength of 62.5 kHz. A recycle delay of 4 s was used. The sample was spinning at a MAS frequency of 8 kHz. A total number of 6240 scans (approximately 7 hrs) were collected for u-ALA RCs, while for 3-ALA, 4-ALA and 5-ALA labelled bacterial RCs around 256 scans (approximately 20 mins) were collected. An artificial line broadening of 30 Hz was applied prior to Fourier transformation. All the ^{13}C-MAS NMR spectra were referenced to the carbonyl resonance of solid tyrosine·(HCl) at 172.1 ppm. A small zero order phase correction was applied to correct line shape asymmetry to the dark and photo-CIDNP spectra of the RCs.

4.2.3 Theoretical models and methods

The coordinates for the initial model of the bacteriopheophytin molecule have been extracted from the 1M3X crystal structure of *R. sphaeroides* WT (Camara-Artigas *et al.*, 2002a). From this crystal structure, bacteriopheophytin *a* of the active

branch with residue id of 855 has been used. This model was partially optimized by relaxing carbons and nitrogens in the porphyrin ring, and all the hydrogen atoms, while fixing the positions of the peripheral carbon atoms. In this way x-ray crystallography and molecular modeling refinement artifacts were corrected by DFT, while preserving the supramolecular structure of the system due to the applied constraints. A DFT model of a fully relaxed BPhe *a* was obtained to mimic the free monomers in solution state. Both geometry optimizations have been carried out in vacuum within the DFT framework with the ADF program (Fonseca Guerra *et al.*, 1998; te Velde *et al.*, 2001; ADF2009.01, 2009) using the Becke's (Becke, 1988) and Lee-Young-Parr's (Lee *et al.*, 1988) gradient-corrected functional (BLYP) in conjunction with a TZP Slater-type basis set.

NMR chemical shifts have also been computed with ADF program. The calculated ^{13}C chemical shifts were referred to calculations performed on TMS and calibrated accordingly. The difference of chemical shifts between the constrained and fully relaxed geometry of the BPhe *a* has been obtained and compared with the experimental observations.

4.3 Results

The origin of the solid state photo-CIDNP effect is now well understood, which makes it applicable for in-depth biophysical investigations (Jeschke & Matysik, 2003; Daviso *et al.*, 2009a). The overview of the photo-CIDNP mechanisms in different RCs is presented in Chapter 2, Figure 2.2. We use different labeling patterns and perform photo-CIDNP on WT RCs under continuous illumination, where the enhancement is established by the combination of the three spin mixing (TSM) and differential decay (DD) mechanisms (Prakash *et al.*, 2005). In the electron-electron-nuclear TSM the symmetry of coherent spin evolution in the spin correlated radical pair is broken by the combined operation of nuclear Zeeman interaction, electron-electron coupling and pseudosecular *hf* coupling (Jeschke, 1997). In the DD mechanism, the symmetry of the coherent spin evolution in the correlated radical pair is broken by different lifetimes of singlet and triplet radical pairs (Polenova & McDermott,

1999). Understanding of these spin-chemical processes allowed to apply photo-CIDNP MAS NMR as an analytical tool for elucidating electronic structures of the special pair (Daviso *et al.*, 2009c). Here we build on these earlier studies and follow a self-consistent approach to assign the Φ_A response and apply photo-CIDNP magic-angle spinning (MAS) NMR to conclude on the characterization of the electronic and spatial structure of the donor-acceptor radical pair state $P^+\Phi_A^-$.

4.3.1 Signal intensity

Figure 4.2 shows ^{13}C MAS NMR spectra of RCs of *R. sphaeroides* WT containing uniformely ^{13}C labelled BChl and BPhe cofactors. The top trace (spectrum A) shows the data for the sample when it is measured in the dark. The signal is very weak and comprises a broad feature around 35 ppm from the aliphatic carbons in the protein. Upon illumination with continuous white light, however, strong emissive signals appear (spectrum B). All light induced signals are emissive and are negative relative to the absorptive spectrum in trace A. The light induced signals appear in spectral regions in which carbons of BChl and BPhe cofactors are resonating. This contrasts with data collected from RCs with ^{13}C at natural abundance (Prakash *et al.*, 2006), where only the response from the aromatic ^{13}C is

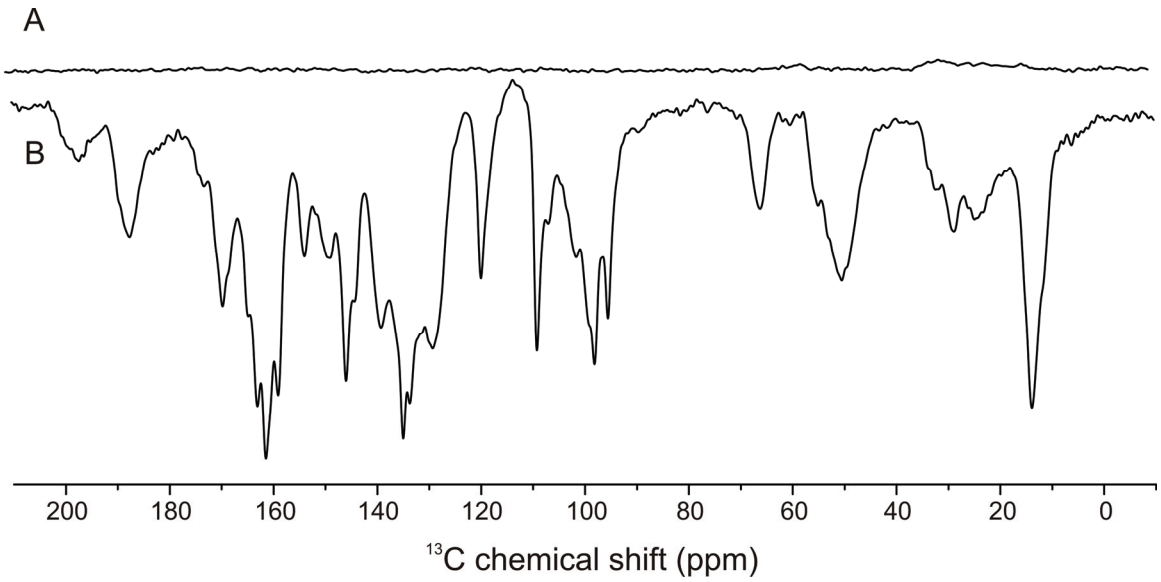

Figure 4.2 One-dimensional ^{13}C photo-CIDNP MAS NMR spectra of u-ALA labelled RCs of *R. sphaeroides* WT (A) in the dark and (B) under continuous illumination with white light. All the spectra have been collected at a magnetic field of 4.7 Tesla and a temperature of 223 K at a spinning frequency of 8 kHz.

enhanced. Obviously, the polarization is spread by spin diffusion within the frozen sample and allows also for enhancement of aliphatic carbons. Even though an increase in signal-to-noise of about one hundred is expected by incorporation of uniformly labelled cofactors, this is not experimentally observed. The overall signal intensity achieved here in samples with cofactors that are uniformly labelled in the macrocycle is significantly smaller than for samples with cofactors containing ^{13}C in natural abundance or samples with sparsely labelled cofactors (Schulten *et al.*, 2002; Prakash *et al.*, 2007; Daviso *et al.*, 2008b).

Although dense labeling opens new channels for spin diffusion and spin-spin relaxation, these effects can be ruled out as sink for intensity as shown by time-resolved experiments using laser excitation immediately before the NMR acquisition (data not shown). Hence, the addition of nuclear spins affects the build-up of nuclear polarization. In a future combined experimental and theoretical study, this phenomenon will be addressed further.

4.3.2 Peak assignments

By using different labeling patterns and by exploiting the additional selectivity offered by the photo-CIDNP mechanism it is possible to address the ground state NMR response with atomic selectivity for the ^{13}C carbons of the rings and the pheripheral side chains of the cofactors involved in the formation of the primary radical pair $P^{+}\Phi_{A}^{-}$. Isotopically labelled RCs prepared from 3-^{13}C-ALA, 4-^{13}C-ALA or 5-^{13}C-ALA substrate in the growth medium have been studied already and provided almost complete chemical shift assignments for signals originating from the donor BChls P_L and P_M, including the peripheral carbons. Here we make the next step, which is to resolve the weak response from the Φ_A from the strong background of the photo-CIDNP signals originating from the Special Pair, which has been partially assigned previously (Schulten *et al.*, 2002; Prakash *et al.*, 2005; Prakash *et al.*, 2006; Prakash *et al.*, 2007; Daviso *et al.*, 2009a).

In Figure 4.3A, the ^{13}C MAS NMR spectrum of u-ALA labelled RCs is shown. The data are aligned with spectra collected from RCs obtained by feeding the 3-^{13}C-ALA, 4-^{13}C-ALA or 5-^{13}C-ALA labelled precursors in the growth medium

for *R. sphaeroides* WT (Figure 4.3 B, C & D). From the spectra a peak list has been compiled consisting of 78 chemical shifts that are sequentially indexed (Table 4.1). Most of the signals from the Special Pair have been already assigned and these are indicated with the dotted lines in Figure 4.3. The peaks indicated by solid lines are attributed to bacteriopheophytin, and the corresponding shifts are given in parenthesis in the table 4.1 along with the index numbers, while table 4.2 presents a self-consistent assignment of the signals that is based on the comparison with solution data, 2D data for RCs reconstituted with plant Pheo *a* and chemical shift calculations.

In Figure 4.3A, in the region between 200 and 180 ppm, four signals are from the carbonyls of the Special Pair cofactors (Chapter 2). The peak at 197.0 ppm with index 1 is attributed to $C3^1$ of the Φ_A and the signal at 188.6 ppm (# 5) is ascribed to $C13^1$ of the Φ_A. The shifts are comparable with the chemical shifts observed for the $C3^1$ (199.2 ppm) and $C13^1$ (189.3 ppm) response from monomeric BPhe *a* in acetone solution and both signals align well with the downfield response from the 3-^{13}C-ALA labelled RCs in Figure 4.3B, where the carbonyl carbons are also labelled (Egorova-Zachernyuk *et al.*, 2008).

The region between 180 and 160 ppm shows two sets of signals that reproduce well across the collection of labelled samples. The 8 strongest signals (# 12 - 19) originate from the Special Pair (Prakash *et al.*, 2007; Daviso *et al.*, 2009a). In the downfield part of the region, 4 relatively weak peaks are discerned, (# 7 - 10) at 174.2, 172.9, 170.7 and 169.3 ppm. These signals match very well with the $C17^3$, C6, C19 and $C13^3$ of the BPhe *a* in solution and with the 2D correlation data collected from a sample reconstituted with uniformly labelled plant pheophytin *a* (Egorova-Zachernyuk *et al.*, 1997; Egorova-Zachernyuk *et al.*, 2008). In addition the peak at 168.2 ppm (# 11) is in line with a previous photo-CIDNP assignment for the C9 of the Φ_A (Daviso *et al.*, 2009a).

In the region between 160 and 140 ppm, most of the response is due to aromatic carbons of Special Pair cofactors P_L and P_M (Prakash *et al.*, 2007; Daviso *et al.*, 2009a). Only the signals with index 20, 24 and 29, are attributed to Φ_A. In the region between 140 and 119 ppm (# 30 - 41), all signals that originate from the

Table 4.1 Complete peak list of NMR ^{13}C chemical shifts with index numbers from u-ALA RCs spectrum (the signals attributed to the Φ_A are given in parenthesis).

index	^{13}C Chemical shift (ppm)	index	^{13}C Chemical shift (ppm)
1	(197.0)	40	126.9
2	195.6	41	119.5
3	193.5	42	108.7
4	189.4	43	(107.5)
5	(188.6)	44	106.6
6	187.5	45	104.1
7	(174.2)	46	103.0
8	(172.9)	47	102.0
9	(170.7)	48	101.2
10	(169.3)	49	100.4
11	(168.2)	50	(99.6)
12	166.5	51	98.3
13	165.9	52	(97.6)
14	164.4	53	(95.1)
15	162.6	54	(65.8)
16	161.0	55	(55.6)
17	160.1	56	54.7
18	158.5	57	52.7
19	157.2	58	(52.5)
20	(154.4)	59	51.7
21	153.6	60	50.9
22	151.5	61	50.0
23	149.8	62	49.1
24	(148.7)	63	48.3
25	148.5	64	47.4
26	145.6	65	46.1
27	144.5	66	(33.6)
28	143.5	67	32.1
29	(141.2)	68	(31.5)
30	138.7	69	29.9
31	137.2	70	29.5
32	136.8	71	28.4
33	136.2	72	(27.2)
34	134.3	73	(24.6)
35	132.8	74	22.6
36	130.8	75	(21.3)
37	129.7	76	19.1
38	128.8	77	(13.5)
39	127.4	78	(11.4)

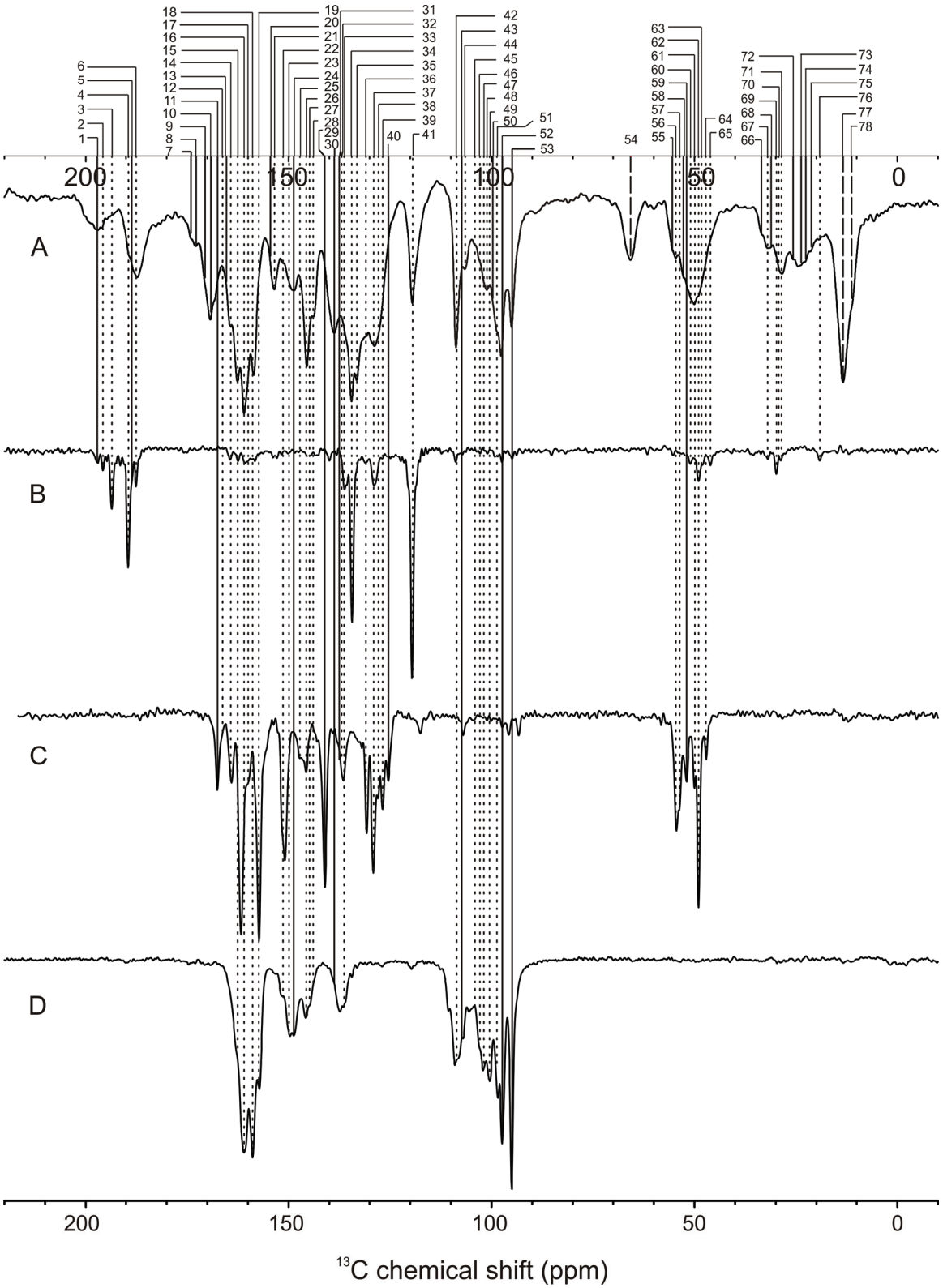

Figure 4.3 A set of one-dimensional ^{13}C photo-CIDNP MAS NMR spectra collected from (A) u-ALA, (B) 3-ALA, (C) 4-ALA, (D) 5-ALA labelled RCs of *R. sphaeroides* WT under continuous light in a magnetic field of 4.7 Tesla and at a temperature of 223 K. The spinning frequency was set to 8 kHz. The dotted lines indicate the responses from P_L and P_M using the assignments obtained in previous work, while the signals from the Φ_A are designated by solid lines. When signals from the P_L, P_M and the Φ_A coincide, their position is indicated with dashed lines.

Special Pair and bacteriopheophytin have been assigned before (Daviso *et al.*, 2009a). The relatively strong response in this region is in line withthe assignments to carbons of the aromatic ring, which is the source of buildup of nuclear spin polarization (Daviso *et al.*, 2009a).

For the region between 110 and 90 ppm four signals can be attributed to the Φ_A. Three of these signals (43, 52 & 53) have been identified earlier (Prakash *et al.*, 2007). The peak at 99.6 ppm (# 50) is ascribed to the C10 (Φ_A). The relatively intense response from the C5 at 97.6 ppm and the C20 at 95.1 ppm confirms that these Φ_A signals are from carbons in the aromatic ring.

In the aliphatic region of the spectrum, the signals at 55.6 (# 55) and 52.5 (# 58) ppm are attributed to the C8 and the C18 of the Φ_A, while the other signals were already assigned from photo-CIDNP MAS NMR data collected from 3-^{13}C-ALA and 4-^{13}C-ALA labelled RCs (Daviso *et al.*, 2009a). The distinct peak at 65.8 ppm (# 54) is assigned to carbon C13^2 from all the cofactors by analogy with data for the BChl and BPhe monomers in solution (Egorova-Zachernyuk *et al.*, 2008). In the region between 40 and 0 ppm, most of the signals, with indices between 66 and 78, are from the Special Pair and were rigorously assigned by 2D DARR experiments from 3-^{13}C-ALA labelled RCs (Chapter.3). The remaining peaks at 33.6, 31.5, 27.2, 24.6 and 21.3 ppm are tentatively assigned to the bacteriopheophytin by comparing with the solution data of BPhe (Egorova-Zachernyuk *et al.*, 2008). Two distinct signals at 13.5 and 11.4 ppm (# 77 & 78) indicated by dashed lines, represent the collective responses from the peripheral carbons C21 and 121 or 82 of all cofactors. The assignments for P_L and P_M are summarized in the tables provided in the appendix.

4.3.3 Electronic tuning of Φ_A in the protein matrix

During electron transfer, the bacteriopheophytin in the active branch forms a radical pair state with the Special Pair. In chapter 2, we learnt that the differences in chemical shifts of the BChl *a* in the Special Pair (P_L and P_M), are very significant, and that the variations in ^{13}C chemical shifts of macrocycles reflect the changes in shape of the macrocycles, the electronic properties of the protein surrounding and

Table 4.2 ^{13}C NMR chemical shifts assigned to BPhe *a* and its monomers in acetone, with respective theoretically calculated chemical shift differences between the monomer and protein-bound BPhe *a*

IUPAC	^{13}C Chemical shift (ppm)					
	Observed shifts of BPhe *a* in Acetone	Observed shifts of BPhe *a* by Photo-CIDNP MAS NMR	Experimental Δσ (solid-liquid)	Theoretically calculated shifts of fully relaxed BPhe *a*	Theoretically calculated shifts of constrained Bphe *a*	Theoretical Δσ (Const-relax)
1	139.7	141.2	1.5	140.7	140.7	0.0
2	138.5	138.7	0.2	149.2	145.4	-3.8
2^1	13.9	13.5	-0.4	17.2	17.0	-0.2
3^1	199.2	197.0	-2.2	201.9	201.4	-0.5
3^2	34.0	33.6	-0.4	35.2	37.8	2.6
4	138.1	137.2	-0.9	142.3	142.6	0.3
5	97.9	97.6	-0.3	100.5	100.4	-0.1
6	172.4	172.9	0.5	173.5	171.3	-2.2
7^1	23.7	24.6	0.9	25.7	26.5	0.8
8	55.4	55.6	0.2	66.0	65.5	-0.5
8^1	30.7	27.2	-3.5	39.6	45.5	5.9
8^2	11.5	11.4	-0.1	13.7	18.5	4.9
9	164.3	168.2	3.9	173.1	175.0	1.9
10	100.2	99.6	-0.6	101.7	100.2	-1.4
12^1	11.5	11.4	-0.1	12.1	13.1	1.0
13	129.2	126.9	-2.3	138.6	137.6	-1.0
13^1	189.3	188.6	-0.7	196.3	193.5	-2.8
13^2	65.5	65.8	0.3	76.3	75.1	-1.3
13^3	170.2	169.3	-0.9	179.4	178.5	-0.9
14	148.7	148.7	0.0	151.6	151.7	0.1
15	110.3	107.5	-2.8	119.3	117.8	-1.5
16	158.7	154.4	-4.3	171.1	170.6	-0.5
17	51.4	51.7	0.3	64.4	62.7	-1.7
17^1	31.3	31.5	0.2	35.3	33.3	-2.0
18	50.9	52.5	1.6	59.3	56.8	-2.5
18^1	22.9	21.3	-1.6	25.6	26.2	0.6
19	171.7	170.7	-1.0	174.4	172.1	-2.3
20	97.2	95.1	-2.1	102.4	101.4	-1.0

hydrogen bonding of *e.g.* the 3^1-acetyl and 13^1-keto carbonyl groups. Figure 4.4A and table 4.2 show the differences in the chemical shift ($\Delta\sigma$) for the Φ_A in the protein matrix relative to BPhe *a* monomer species in acetone. There are little changes in electron density in rings I and III, while for rings II and IV there are cumulative negative shifts. Significant $\Delta\sigma$'s for the $C8^1$, C9 and C16 atoms are around ~ 3.5 ppm and for the $C3^1$, C13, C15, and C20 the $\Delta\sigma$ ~ 2.0 ppm. The small changes in electron density in rings I and III indicate a planar ring conformation and a stable configuration with distinct pyrrole and pyridine nitrogen atoms in the bacteriopheophytin *a*, as opposed to the much softer and distorted bacteriochlorophyll ring system with the coordinated Mg^{2+} ion in the center that is subject to polymorphism, dynamics and electrostatic polarization (Chapter 2). Since the pheo is involved in the cascade of symmetry breaking events in the RC, and symmetry breaking is related to structural distortions in the ground state, the data indicate that the primary source of the symmetry breaking is in the deformation of P, while the extent of protein induced deformation of the BPhe *a* molecule appears much less (Pandit *et al.*, 2010; Wawrzyniak *et al.*, 2011). The deformation of the Φ_A has been analyzed with theoretical calculations, where the electronic structures of the bacteriopheophytin molecule in a completely relaxed state and in the protein matrix with constraints were computed. Figure 4.4B shows that the $\Delta\sigma$ from these calculations are similar and match the experimental observations. When a completely relaxed BPhe *a* from computer modeling is overlaid with BPhe *a* from the X-ray data for the bacterial RC (Figure in Appendix-B), the structural differences are small, within 0.2 Å. For the peripheral region the differences are larger, and produce chemical shift differences up to 10 ppm, in line with the experimental data (Table 4.2). In particular the conformation of the ethyl substituent on $C8^1$ and $C8^2$ appears affected.

Finally, an electrochemical investigation of the redox properties of bacteriopheophytin *a* in aprotic solvents was performed by cyclic voltammetry to determine the midpoint potential, which is -0.65 V with respect to the normal hydrogen electrode (Cotton & Van Duyne, 1979). This is very close to the experimental midpoint potential of -0.63 V determined for the BPhe *a* in both

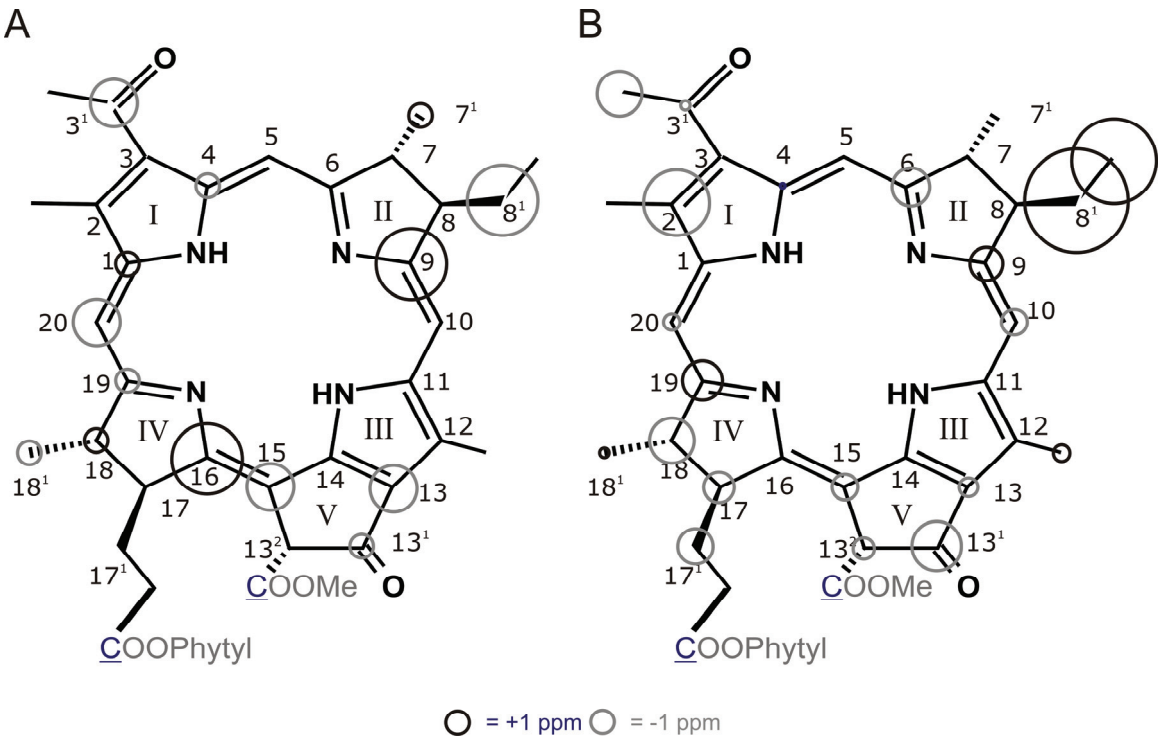

Figure 4.4 Relative electron densities of bacteriopheophytin (Φ_A) in the electronic ground state derived (A) experimentally from the chemical shift differences between BPhe *a* in solution in acetone and BPhe *a* cofactor in RC and (B) Theoretically calculated chemical shift differences between fully relaxed structure and constrained optimized structure of BPhe *a* from the x-ray structure from 1M3X (Camara-Artigas *et al.*, 2002b).

active and inactive branch in the protein (Woodbury & Parson, 1984; Noy *et al.*, 2006). This implies that the redox potential of the BPhe cofactor present in the protein matrix is only marginally affected by the surrounding environment.

This matches very well with our observation that the structure of the Φ_A is very similar to the structure of BPhe *a* in solution, with little evidence for packing effects from the protein matrix. We thus conclude that the BPhe of the active branch is not tuned in a special manner by its surroundings and represents an electron sink due to its redox potential that is different from P. A similar conclusion has been made for the subsequent cofactor namely the Quinone acceptor Q_A in RCs that they remain in the same orientation even upon illiumination light by ENDOR experiments (Flores *et al.*, 2010). Taking together, the cofactors in the active branch appear to be the same under normal conditions.